PERGAMON

Journal of Structural Geology 24 (2002) 1087–1099

JOURNAL OF STRUCTURAL GEOLOGY

www.elsevier.com/locate/jstrugeo

Interaction of flexural shear, *S–C* fabrics, and oblique shear during folding of micaceous quartzite

J. Hippertt[a,*], E. Tohver[b]

[a]*Departmento de Geologia, Universidade Federal de Ouro Preto, 35400-000, Ouro Preto, MG, Brazil*
[b]*Department of Geological Sciences, University of Michigan, Ann Arbor, MI 48109, USA*

Received 1 December 2000; revised 1 June 2001; accepted 1 June 2001

Abstract

This paper investigates the geometry, microstructure, and *c*-axis fabrics of an outcrop scale, micaceous quartzite fold produced under greenschist facies metamorphic conditions in the Moeda quartzite, Quadrilátero Ferrífero granite–greenstone terrain, southeastern Brazil. The fold limbs show development of opposed *S–C* fabrics and asymmetric quartz *c*-axis fabrics compatible with flexural slip along the fold surface. Towards the fold hinge, there is an increasing presence of oblique shear bands (here named *S-bands*) which gradually change to crenulations within the hinge zone. The oblique *S*-bands are interpreted to have formed through connection of several *S*-planes, increasing accommodation of antithetical shear along these *S*-planes and offset of the initial *C*-planes at intermediate stages of folding. This mechanism represents a kinematic inversion in the role played by the two sets of foliations in *S–C* structures. Our observations support flexural slip for early stages of folding. However, with progressive closure of the fold, the flexural slip mechanism involves increasing contributions from oblique shear on the *S*-bands, thus approximating an intermediate situation between flexural slip and passive folding (shear parallel to the axial plane). © 2002 Published by Elsevier Science Ltd.

Keywords: Flexural shear; *S–C* fabrics; Folding

1. Introduction

Folding of rocks is well-documented in modern structural geology. The most commonly cited folding mechanisms are orthogonal flexure, volume-loss flexure, passive folding, flexural flow, and flexural slip. Orthogonal flexure, referred to as tangential–longitudinal strain by Ramsay (1967), involves the partitioning of compressional and tensile stresses in relation to a neutral surface, the area of which remains constant throughout folding. This mechanism is characteristic of folds with low curvatures developed in competent materials, and is indicated by the presence of extensional structures in the convex side, and compressional structures in the concave side of the fold (Twiss and Moore, 1992, p. 240). Volume-loss folding (Groshong, 1975) involves the selective removal or transfer of material resulting in a change in the overall geometry of the deformed body. Passive folding, also referred to as slip folding or shear folding (Ramsay, 1967), involves shear along planes parallel to the axial plane of the fold, with the hinge-zone moving relative to the limbs. In this mechanism, folding can occur by dissolution (Groshong, 1975), with or without associated slip along axial-plane-parallel surfaces (e.g. Williams and Jiang, 1999), with or without shortening normal to the axial plane, or by a combination of all these processes (Bell and Hickey, 1997). Both flexural flow (e.g. Henderson et al., 1986) and flexural slip (Donath and Parker, 1964; Chapple and Spang, 1974; Ramsay, 1974; Tanner, 1989) are commonly envisioned as the bending of a card deck, with folding accommodated by slip along independent shear planes parallel to the fold surface. The sole difference between these two folding mechanisms lies in the thickness of the 'cards' themselves; flexural slip provides for discrete slip planes (e.g. bedding surfaces) separating layers of finite thickness, whereas flexural flow involves a more homogeneous shear along vanishingly thin 'cards'. Fig. 1 summarizes these 'end-member' mechanisms, and combinations of them are commonly used to explain folding of rocks. However, fold development in rocks is unlikely to follow a single end-member path, as the mechanisms of strain accommodation vary spatially and temporally during the development of a fold (e.g. Bell, 1986; Davis and Forde, 1994; Hudleston et al., 1996; Williams and Jiang, 1999).

Folding mechanisms are generally inferred from both

* Corresponding author. Tel.: +55-31-3559-1600; fax: +55-31-3559-1606.
E-mail address: hippertt@degeo.ufop.br (J. Hippertt).

0191-8141/02/$ - see front matter © 2002 Published by Elsevier Science Ltd.
PII: S0191-8141(01)00093-1

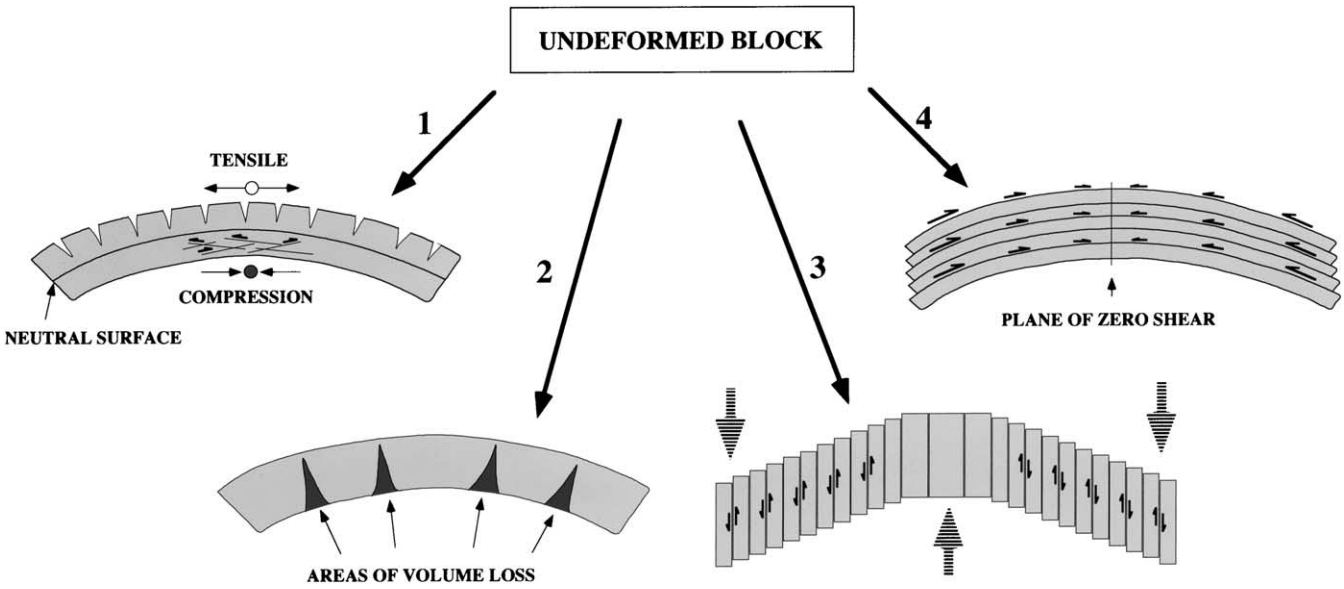

Fig. 1. Sketch summarizing the most commonly invoked kinematic models of folding: 1. orthogonal flexure; 2. volume loss folding (a material dependant fold mechanism); 3. passive folding (also referred to as slip folding) and; 4. flexural slip/flow (with tangential–longitudinal strain operating between the individual slip planes).

whole-fold geometries (e.g. Hudleston and Lan, 1993; Hobbs et al., 2000) and other macroscopic features such as cleavages (e.g. Borradaile, 1978; Treagus and Treagus, 1992), internal faulting (e.g. Tanner, 1992) and patterns of vein occurrence (e.g. Henderson et al., 1986). A hinge-zone that is thick and richer in quartz compared with the limb zone is interpreted as volume-transfer from the limb to the hinge. Tanner (1989) used observations of imbricate structures such as strike-slip duplexes and slickenfiber distribution patterns to confirm shear between individual layers of a fold. Inferences about fold mechanisms have also been made through the distribution of stylolites as well as strain recorded by other bodies of known pre-deformational shape such as oolites (e.g. Groshong, 1975). In addition, information on the operative folding mechanism can be deduced from the microstructure through investigation of porphyroblasts (e.g. Bell and Hickey, 1997; Johnson, 1999; Williams and Jiang, 1999) and grain-scale deformation mechanisms (Chapple and Spang, 1974; Carreras et al., 1977; Stünitz, 1991).

This paper presents a microstructural analysis of a low-greenschist facies micaceous quartzite fold. This fold was selected for structural investigation because of the overall symmetry of the fold geometry, the symmetry of microstructures within the fold with respect to the overall fold geometry, and the simplicity of its mineralogy. These aspects make this fold a good laboratory for the study of deformation mechanisms involved during folding at low-grade metamorphic conditions. The observation of *S*–*C* fabrics within this fold is consistent with an early stage of folding by flexural slip. However, other microstructures are not consistent with any of the four mechanisms cited above. A new folding mechanism is then presented by which alignment of *S*-foliations developed during flexural slip can lead to the subsequent activation of oblique shear, which allows continued folding.

2. Geological setting

The Moeda quartzite is one of the main Proterozoic units at the base of the metasedimentary Minas Supergroup in the Quadrilátero Ferrífero granite–greenstone terrain. This unit mainly consists of micaceous quartzites (mica content 5–50%), intercalated with varied proportions of more micaceous layers (phyllites/phyllonites). These micaceous quartzites are folded within regional-scale synclines that anastomose around the granitic–gneissic domes of the Quadrilátero Ferrífero (Fig. 2a and b). The reader is referred to Chemale et al. (1994) for an extensive description of the metamorphic-structural setting of this region. The contact between the gneissic domes and the basal supracrustal rocks, as well as the contacts between the major metasedimentary units, have been intensely mylonitized.

Fig. 2. (a) Simplified geological-structural map of the Quadrilátero Ferrífero region, where location of the N–S profile shown in (b) is indicated. (b) Cross-section through the Dom Bosco syncline showing the main supracrustal units and kinematics of the contact shear zones. Numbers annotating the *S*–*C* sketches indicate the angle between *S*- and *C*-planes. Location of the outcrop shown in (c), where the investigated fold sample was collected, is indicated. (c) Outcrop sketch of the contact between banded iron formation (BIFs) and a metasedimentary unit of quartzite/phyllites. The boxed area shows location of the sampled quartzite fold. The measured fold axis (lines with dots) are indicated. (d) Structural data measured at the outcrop shown in (c) and others nearby.

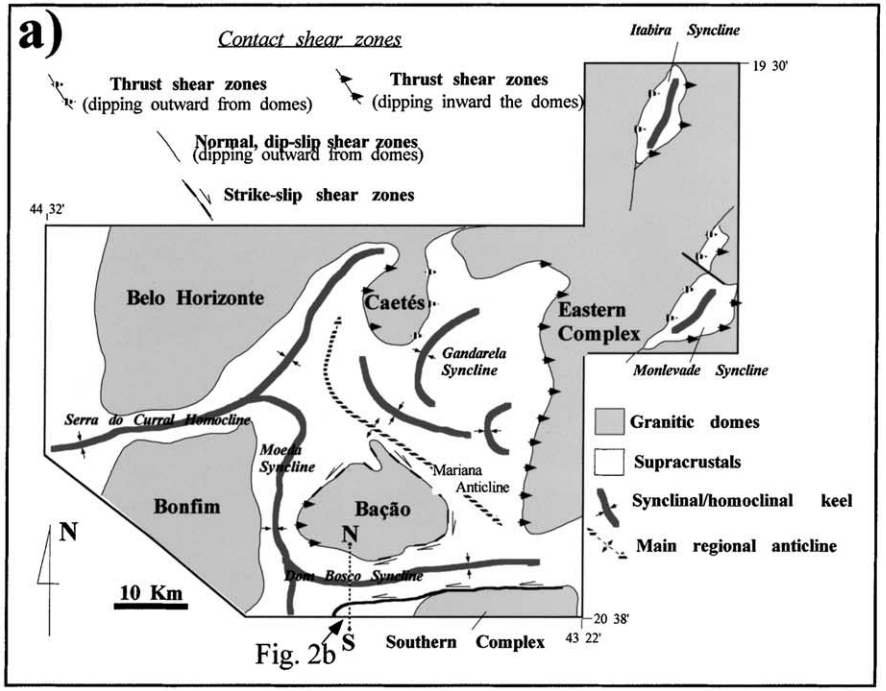
a)
Contact shear zones
Thrust shear zones (dipping outward from domes)
Thrust shear zones (dipping inward the domes)
Normal, dip-slip shear zones (dipping outward from domes)
Strike-slip shear zones
Itabira Syncline
19 30'
44 32'
Belo Horizonte
Caetés
Eastern Complex
Gandarela Syncline
Monlevade Syncline
Serra do Curral Homocline
Moeda Syncline
Mariana Anticline
Bonfim
Bação
N
10 Km
Dom Bosco Syncline
20 38'
43 22'
Southern Complex
Granitic domes
Supracrustals
Synclinal/homoclinal keel
Main regional anticline
Fig. 2b
S

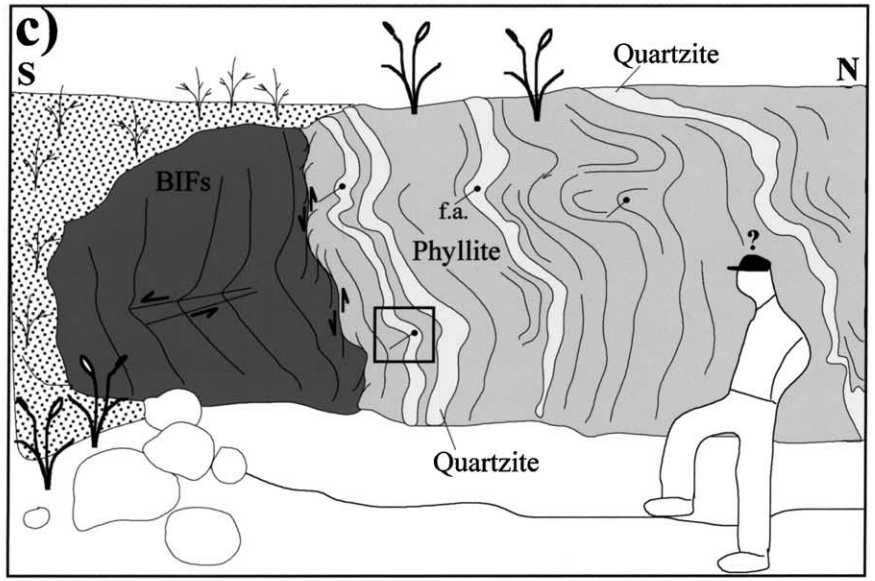
c)
S
N
Quartzite
BIFs
f.a.
Phyllite
?
Quartzite

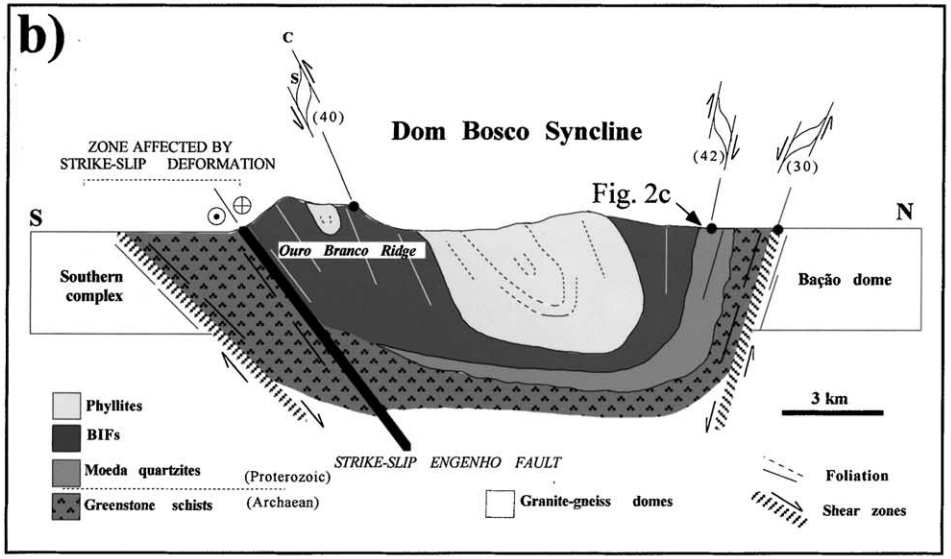
b)
C
S
(40)
Dom Bosco Syncline
ZONE AFFECTED BY STRIKE-SLIP DEFORMATION
(42)
(30)
Fig. 2c
S
N
Ouro Branco Ridge
Southern complex
Bação dome
3 km
Phyllites
BIFs
Moeda quartzites
(Proterozoic)
Greenstone schists
(Archaean)
STRIKE-SLIP ENGENHO FAULT
Granite-gneiss domes
Foliation
Shear zones

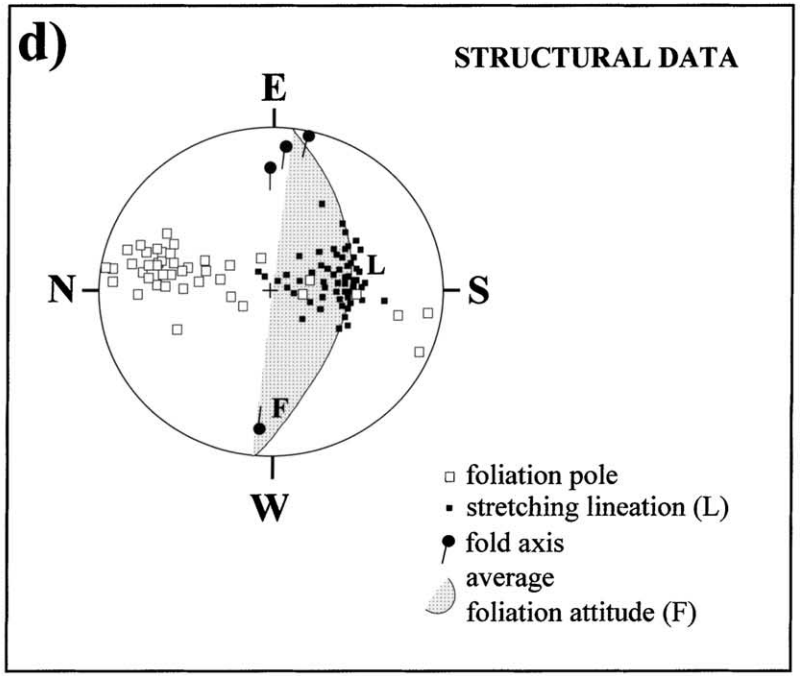
d)
STRUCTURAL DATA
E
N
S
W
L
F
foliation pole
stretching lineation (L)
fold axis
average foliation attitude (F)

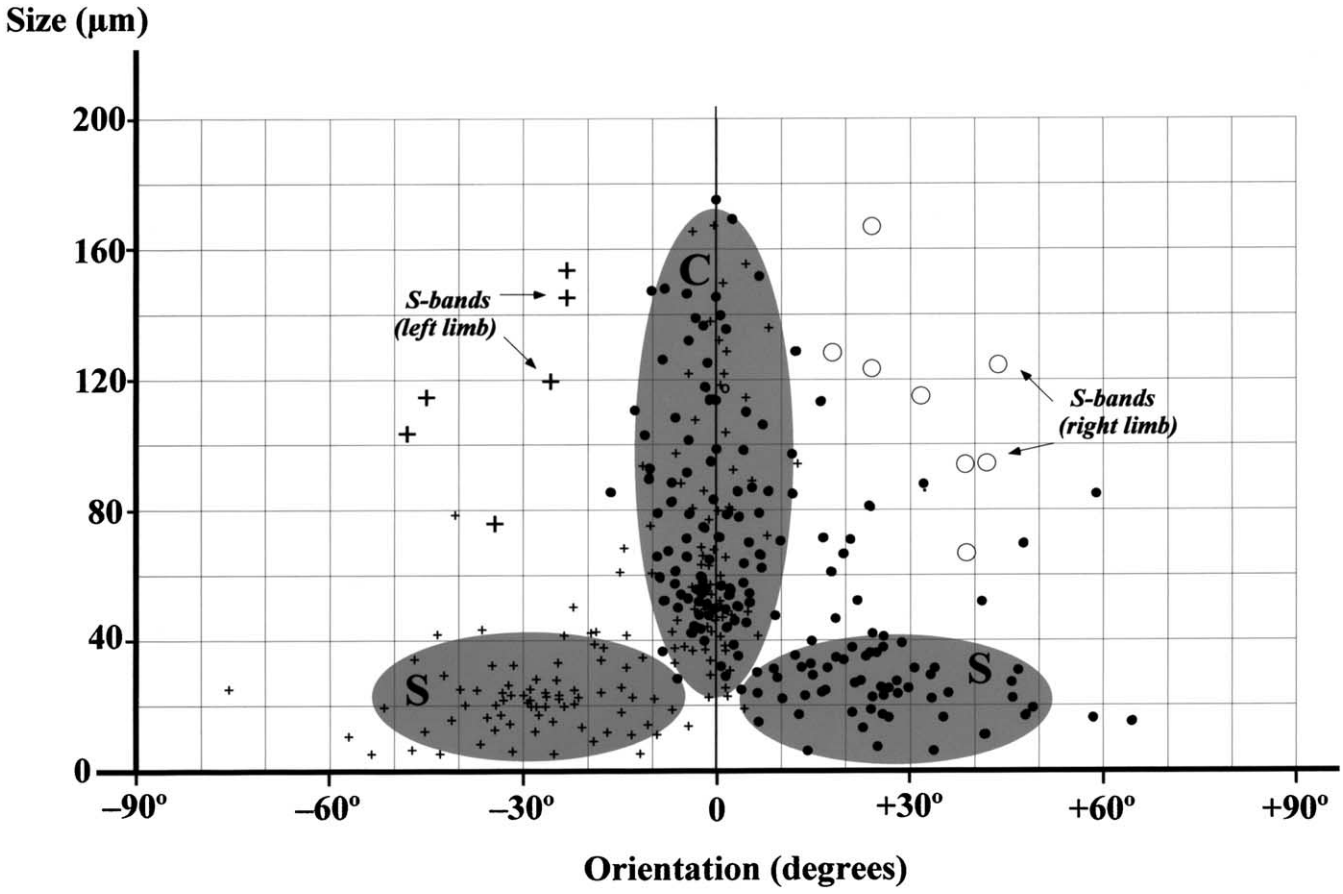

Fig. 3. Orientation (angle to the sedimentary layering) vs. grain size (short morphological axis) of mica crystals in the fold limbs. Crosses represent measurements in the left limb, circles measurements in the right limb, relative to the view shown in Fig. 4a. Large crosses and large circles represent micas from *S*-bands in the respective limbs.

Deformation in these contact shear zones is associated with millimeter- to decimeter-scale folding of the supracrustal rocks in low-strain domains within the shear zones, or in domains immediately adjacent to it. Shear deformation and associated folding occurred under greenschist facies conditions in the presence of fluid, and through operation of different competing deformation mechanisms such as fracturing in feldspar, and solution transfer and crystal-plastic deformation in quartz (Hippertt, 1998). Mass transfer of silica out of the shear zones has produced volume loss and mica enrichment (phyllonitization) in these domains (Hippertt, 1994).

Both open and isoclinal folds are common in the Moeda quartzites deformed in the contact zones. The latter generally display an intrafolial character, and may appear as isolated hinge zones in mica-rich domains. The folds are generally better developed in the domains showing a regular alternating sequence of quartzose and mica-rich layers, where strong strain partitioning has favored folding of the more competent quartz-rich layers, whereas slip on basal planes of mica seems to have accommodated shearing in the more micaceous layers, inhibiting fold development in these domains. Fig. 2c shows an outcrop sketch where the investigated fold was collected. The fold axes are generally at a high angle to the pervasive dip-plunging stretching lineation of the sheared Moeda quartzites (Fig. 2d).

Fig. 4. Plate showing microstructures observed on different domains of the investigated fold. (a) Sketch of the fold. The frontal plane (in black) is the plane perpendicular to the fold axis (F.A.), where thin sections were made. This is also the plane of the outcrop view shown in Fig. 2c. All microstructures are shown in this plane. 'L' denotes mineral lineation. Locations of the microstructures shown in this plate are indicated. (b) Microstructure in the transition between limb and hinge zones. Two sets of opposing oblique foliations (thin white lines) appear to occur relative to the folded main foliation (thick white line), suggesting absence of a consistent flexural shear in these domains. (c) and (d) Microstructures in the left and right limbs, respectively. *S*–*C* fabrics are well developed and indicate opposite shear senses in each limb consistent with flexural slip/flow mechanisms. The shear plane (*C*) corresponds to the main foliation defined by muscovite-rich planes parallel to the sedimentary layering. The oblique foliation (*S*) is defined by thinner muscovite flakes. (e) Detail of an incipient oblique *S*-band oriented at low angle to the *S*-foliation, on the left limb. Relative displacements of the main foliation (white lines) indicate an opposite shear sense relative to the flexural shear on the left limb. All photos (XPL) have the same orientation relative to the sketch in (a).

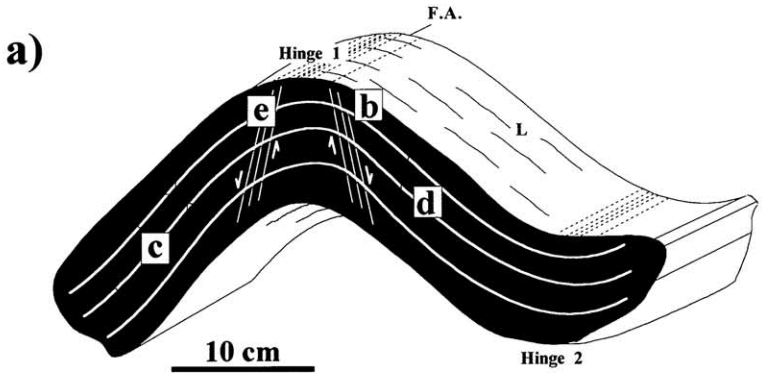
a)
F.A.
Hinge 1
e
b
L
d
c
10 cm
Hinge 2

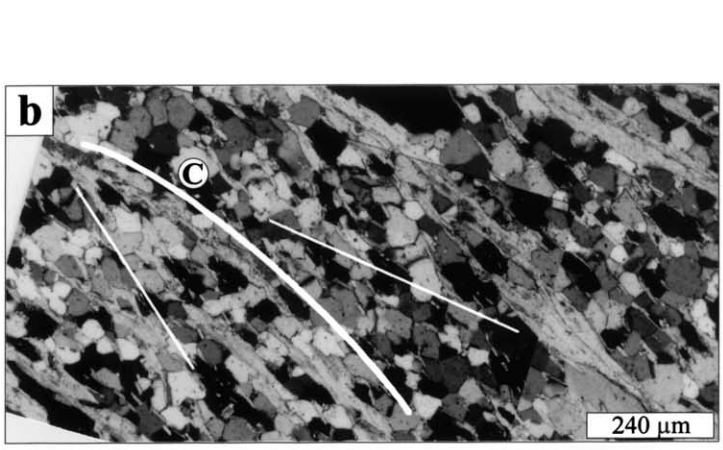
b
C
240 µm

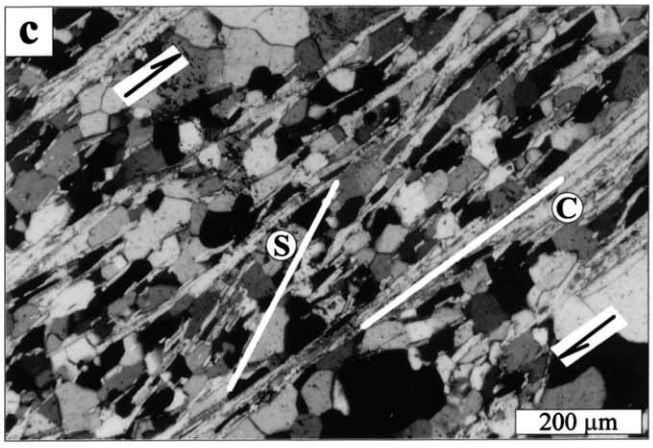
c
S
C
200 µm

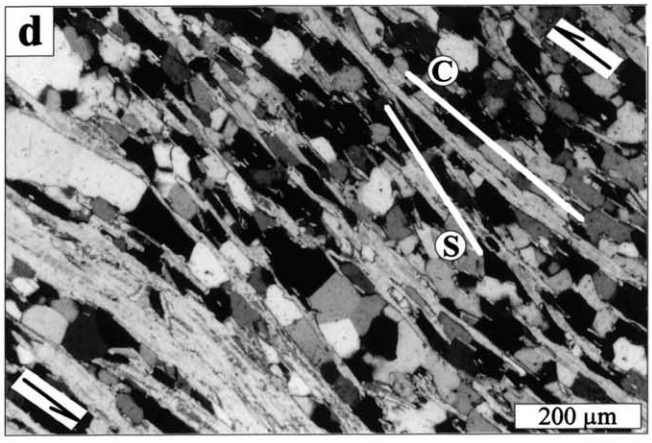
d
C
S
200 µm

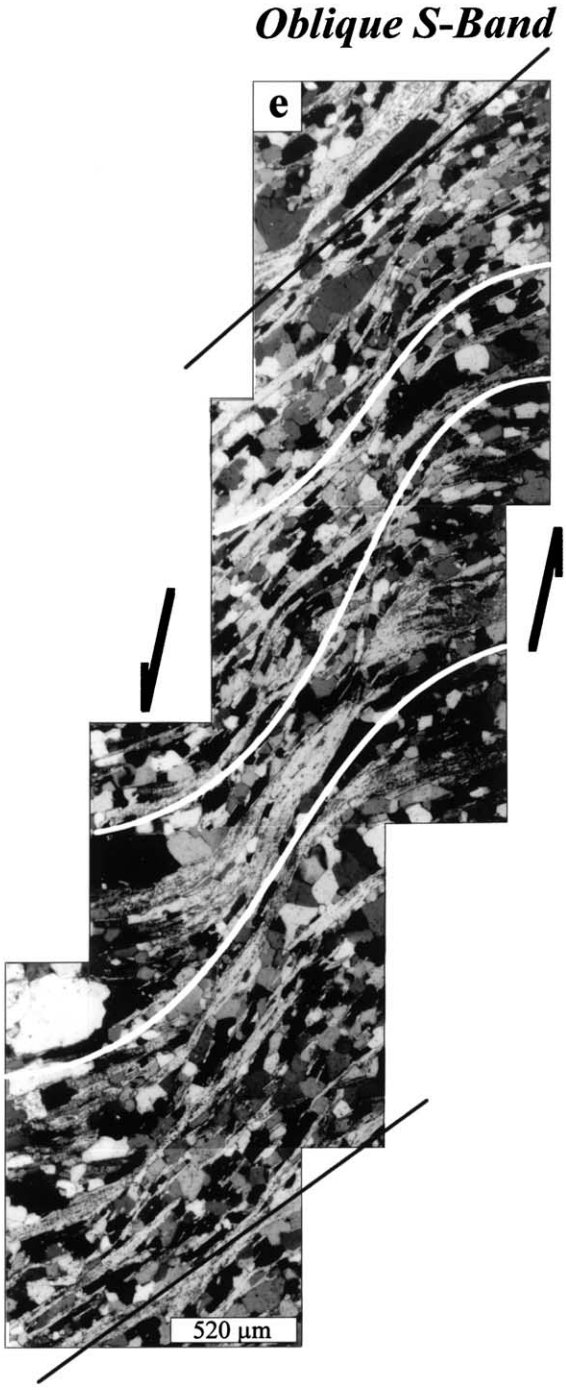
Oblique S-Band
e
520 µm

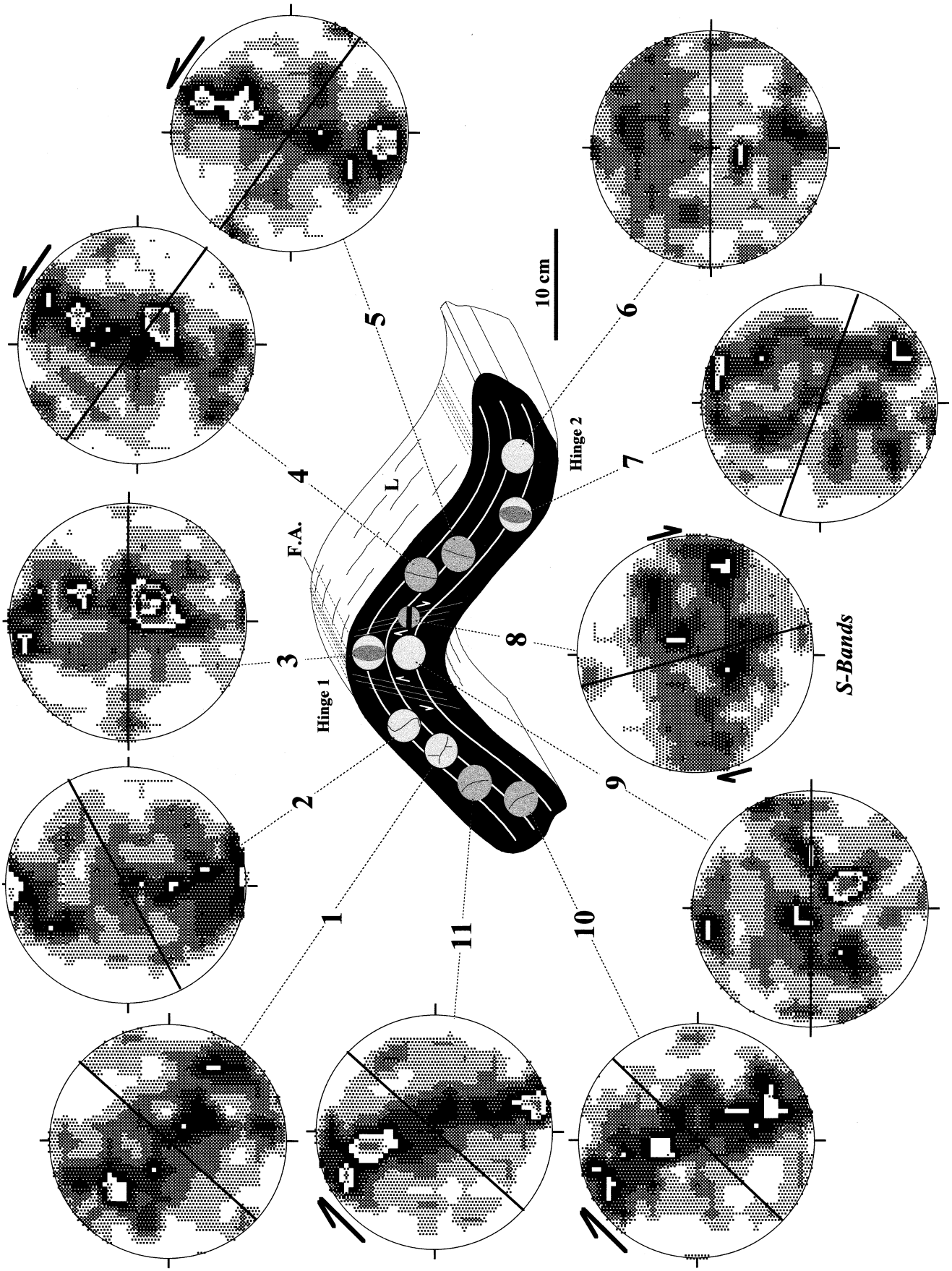
10 cm
F.A.
L
Hinge 1
Hinge 2
S-Bands
1
2
3
4
5
6
7
8
9
10
11

3. Fold description

3.1. Composition and geometry

The folded quartzite layer consists of approximately 40% muscovite and 60% quartz. Quartz occurs as both relic porphyroclasts (30% by volume) and polygonal, recrystallized grains (70% by volume, average size 70 μm). Core-and-mantle structures on quartz porphyroclasts are common. Muscovite occurs as optically weakly-strained flakes showing a bimodal size distribution (maxima at 30 and 135 μm). The sedimentary bedding in the sample is defined by continuous quartzose layers containing relic quartz porphyroclasts with individual beds varying in the amounts of quartz and its average grain sizes. There is no apparent difference in the distribution and volumetric proportion of quartz porphyroclasts in different parts of the fold along a given quartzose layer, suggesting the absence of substantial finite strain heterogeneities between hinge and limb. The main foliation, which is folded around the outcrop-scale folds, is parallel to the sedimentary bedding, and appears as an alternating sequence of mica-rich and quartz-rich domains with an average spacing of 220 μm between two consecutive mica-rich layers. In the investigated fold, orthogonal thickness is uniform and nearly equivalent from limb to hinge. Dip isogons converge on the concave side of the fold and axial-trace thickness increases from hinge to limb. Applying the classification scheme of Twiss (1988) gives a broad aspect ratio of 0.32 and a bluntness of 0.34, characterizing the fold as subangular. The fold is open based on an interlimb angle of 105°. Bulk shortening of the fold sample is approximately 20%.

3.2. Fold fabrics

The types of fabrics observed in this fold vary from limb to hinge, and differ from fabrics present in the unfolded domains. The domains away from the hand specimen- and outcrop-scale folds display a bedding-parallel foliation dispersed around a single orientation maximum. In contrast, in the fold limbs, *S*–*C* fabrics are present as defined by alignment of mica grains in two different orientations (Fig. 3), with the *C*-foliation much more prominent than the *S*-foliation. These two foliations are pervasive in the fold limbs, and appear similar to the type-II *S*–*C* structures of Lister and Snoke (1984). The *S*-foliation, which is defined by the smaller mica grains, is oriented at 15–45° to the prominent *C*-foliation, which is parallel to the original sedimentary bedding and defined by alignment of the largest mica grains. The two limbs show contrary shear senses as indicated by the orientation of *S*-foliations (Fig. 4c and d). The right limb has undergone sinistral shear and the left limb dextral, relative to the view in Fig. 4a. Both shears correspond to a relative movement in which the outer parts of the fold move toward the hinge zone (Fig. 4c and d). This sense of movement, which is obvious in the inflection point of limbs, becomes progressively obscured towards the hinge-zone (Fig. 4b).

Between the fold hinge and *S*–*C* foliated limbs there is a profusion of mica-rich shear bands, herein termed *S-bands*, oriented parallel to the local *S*-foliation, generally on a scale visible with a hand lens. Fig. 4e shows an example of an *S*-band as seen in a thin section made from this intermediate zone between hinge and limbs. These bands, which vary in length from 800 μm to several centimeters, display a consistent orientation with respect to the hinge plane of the fold, depending on which side of the fold they lie. The presence of continuous fine-grained quartz domains displaced across the *S*-bands confirms that they are shear bands (Fig. 4e). The angle between these bands and the axial plane varies with distance from the hinge plane, being approximately 45° immediately adjacent to the hinge plane and decreasing consistently towards the limbs until it is subparallel to the axial plane of the fold. Since the *S*-bands are mineralogically similar to, and always parallel to the local *S*-foliation, they are interpreted as having resulted from the alignment and connection of several *S*-foliations. These bands become less common towards the limbs, where they occur in a less-developed state. The fold hinge is characterized by a triangular zone where no *S*-bands are found (Fig. 4a). Within this triangle, there are no consistent indicators of shear-sense and the rock fabrics change from a typical *S*–*C* fabric to a closely spaced crenulation, the axial plane of which is at low angles to the axial plane of the fold. In the hinge zone, there are also some examples of angular chevron folds formed at the scale of a few mica grains.

At the hand-sample scale, there is a well-developed mineral lineation defined by alignment of mica flakes on the mica-rich layers. This lineation is perpendicular both to the main fold axis and to a closely-spaced crenulation visible in the hinge-zone. The mineral lineation is visible on both the convex and concave surfaces of the fold, but it is most clear on the limbs of the fold, where it is perpendicular to the fold axis. This lineation is less distinct on the top surface of the hinge and is almost completely obscured on the bottom hinge surface by the crenulation. The axial plane

Fig. 5. *c*-Axis fabrics of recrystallized quartz grains (grain size 50–100 μm) measured in different domains of the investigated fold. Relatively sharper, asymmetric single girdle fabrics (diagrams 4, 5, 10 and 11) occur with opposing asymmetries in the fold limbs. More diffuse fabrics (diagrams 2, 3, 6, 7 and 9) appear toward the hinge zones. The recrystallized quartz grains present on the *S*-bands show a diffuse fabric (diagram 8), whose asymmetry is also consistent with the inferred antithetic shearing on the *S*-bands. $N = 250$, lower hemisphere, equal area stereoplots and density contours of 1%/1% area in all diagrams.

of this crenulation is parallel to the axial plane of the main fold, suggesting that it represents a smaller-scale parasitic feature.

3.3. c-Axis fabrics

Fig. 5 shows the domainal quartz *c*-axis fabrics obtained in different quartz-rich layers of the fold and at different distances from the hinge. Overall, the fabric intensities are relatively weak as commonly happens when substantial amounts of a weaker mineral phase are present (e.g. Starkey and Cutforth, 1978). This suggests that deformation mechanisms other than quartz crystal–plasticity (e.g. slip on mica basal planes) contributed to the strain accommodation during progressive folding. However, a preferential orientation of *c*-axes defining asymmetric single girdles or type-I asymmetric cross girdles (Lister et al., 1978) is present, particularly on the fold limbs, and in domains where the mica content is smaller. These fabrics show opposing asymmetries in the different limbs. In contrast, much weaker fabrics occur towards the hinge zones, no asymmetry being observed in the fabric skeletons. Some of the hinge-zone fabrics show a more symmetrical distribution of *c*-axes around the foliation pole, indicative of predominant coaxial deformation in these domains (Law et al., 1990). In the intermediate zone, where the oblique *S*-bands occur, the overall domainal fabrics obtained in the individual quartz-rich layers are always very weak and show no clear asymmetry. However, the quartz aggregates from different layers affected by one specific *S*-band show relatively well-developed asymmetric fabrics in relation to the *S*-band plane, suggesting that these domains were loci of oblique simple shear (see the example shown in Fig. 5). The asymmetry of the *S*-bands is opposite on the different limbs. Within the same limb, the sense of shear in the oblique *S*-bands is always antithetic relative to the shear along the folded quartz-rich sedimentary layers, inferred from *S*–*C* fabrics.

4. Discussion

Flexural slip is a widely invoked mechanism for fold development, where strain is generally considered to have been wholly accommodated at the boundary between competent and incompetent layers (Ramsay and Huber, 1987). Researchers investigating large-scale synclines or anticlines have indentified the occurrence of slip planes along sedimentary bedding planes at intervals ranging from centimeters to tens of meters (Johnson and Page, 1976; Tanner, 1989, 1992). This mechanism presumes that strain is largely accommodated on the slip planes parallel to the folded surface, although the material between the slip planes must also deform via a process dominated by tangential longitudinal strain (e.g. Hudleston et al., 1996). Like flexural slip, flexural flow assumes opposing shear senses within the opposing fold limbs with overall strain diminishing towards the hinge-zone. The principle difference lies in the homogeneously distributed shear invoked by flexural flow versus discrete slip planes in flexural slip. Our findings indicate that strain in the limbs of the investigated fold was accommodated by flexural slip at the level of individual sedimentary beds of centimeter/millimeter scales, leading to development of pervasive *S*–*C* fabrics.

S–*C* fabrics are known to accommodate non-coaxial strain via synthetic shear along *C*-planes and antithetic shear along *S*-planes (Krohe, 1990), with the obliquity of the *S*-planes reflecting the overall shear sense. The geometry of *S*–*C* fabrics in the studied fold suggests that a component of simple shear has occurred along the planes parallel to the sedimentary bedding. The shear senses indicated by the *S*–*C* structures are consistent with the flexural slip model, which predicts the opposing senses of movement observed in each limb. This interpretation is also supported by the increasing asymmetry of single-girdle *c*-axis fabrics towards the limbs, indicating that an increasing component of simple shear (Law et al., 1990) was accommodated away from the hinge zone. The stronger development of the stretching lineation in the limbs, and its orientation perpendicular to the fold axis, are also indicative of flexural slip in these domains. Within the hinge zone, both the microchevrons/crenulations and the more symmetric *c*-axis fabrics suggest a higher component of coaxial deformation (flattening) in this domain. We argue that oblique shear along *S*-bands accommodated strain in the transition zone between the hinge and the limb domains. Evidence for this oblique shear is provided by the offset of the quartzose layers and the presence of relatively well-developed asymmetric *c*-axis fabrics in the *S*-bands.

The flexural slip mechanism provides for a gradual decrease in shear strain as the hinge plane is approached (Ramsay, 1967, p. 392). Interestingly, despite the observed domainal microstructure along the fold, we did not find evidence for significant contrasts of local finite strain between hinge and limbs. This is indicated, for example, by the lack of detectable differences in relic porphyroclast populations from limb to hinge along a given sedimentary bedding plane as well as by the lack of any systematic variation in the angle between the *S*- and *C*-planes in different fold domains. Progressive shear along *C*-planes is expected to be accompanied by rotation of *S*-planes towards the *XZ* plane of the local finite strain ellipsoid (Berthé et al., 1979). Therefore, continued flexural slip in the limbs during progressive fold closure would be expected to produce smaller angles between *S*- and *C*-foliations towards the inflection point of the limbs. Lack of this variation indicates that *S*-plane rotation did not accompany the progressive closure of the fold via flexural slip, and that another mechanism (oblique shear along both the *S*-bands and individual *S*-foliations) may have accommodated strain at intermediate stages of folding. The parallelism between *S*-foliations and *S*-bands as well as the merging of individual

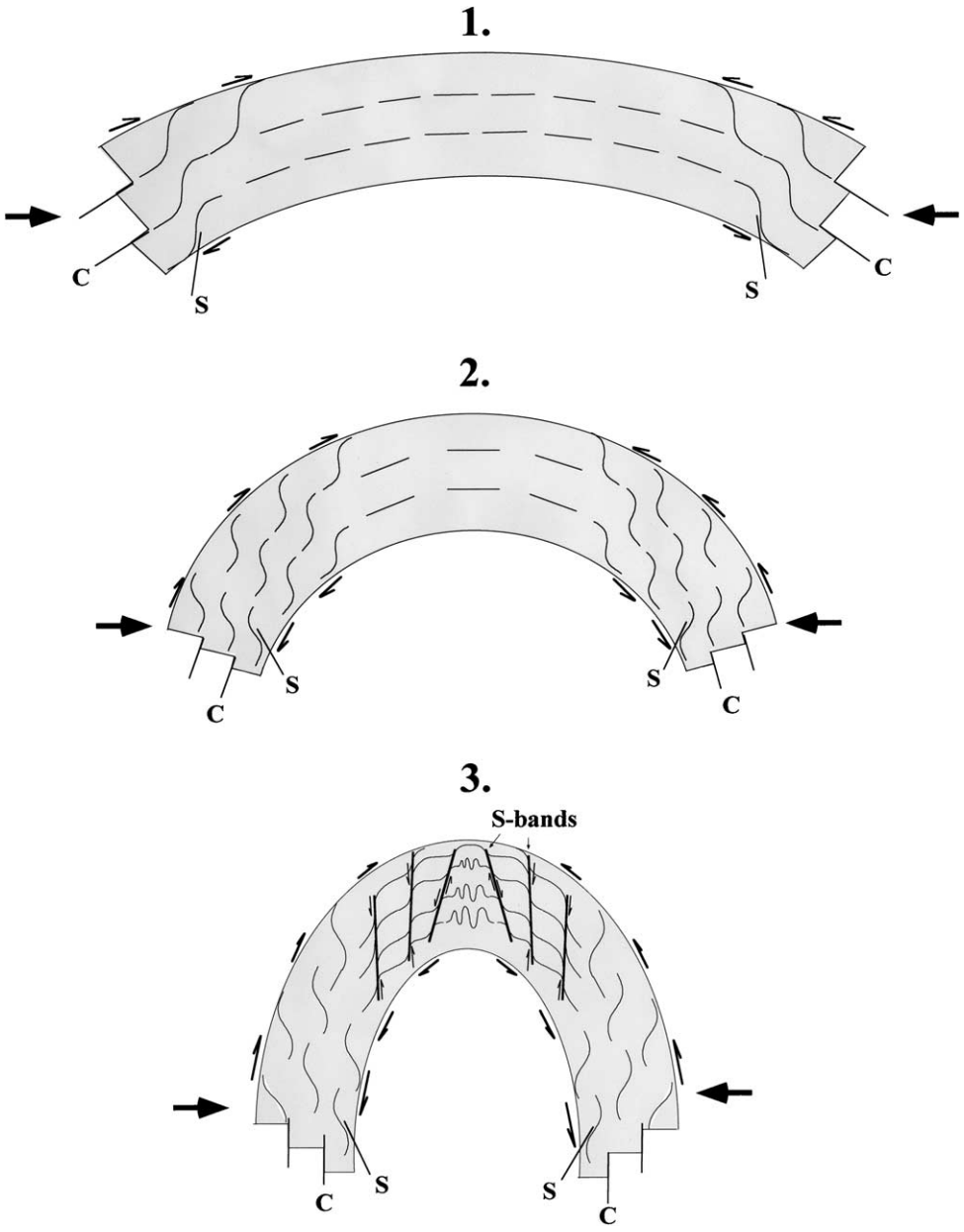

Fig. 6. Suggested sequence of progressive folding with development of *S*–*C* fabrics due to flexural shear in the fold limbs (stages 1 and 2). At more advanced stages of folding (stage 3), connection of *S*-planes leads to development of oblique *S*-bands at the intermediate zones between limbs and hinges, where antithetical shear (relative to the flexural shear in the corresponding limb) is accommodated. These *S*-bands disrupt the earlier formed *C*-planes and accommodate the majority of strain in these domains.

mica grains from *S*-foliations into the *S*-band suggests a scale-invariant relationship, in which *S*-bands are a larger scale version of *S*-foliations (Davis and Forde, 1994; Hippertt, 1999). The *S*-bands are interpreted to have formed through the alignment and subsequent connection of various micaceous *S*-planes across different sedimentary layers (Fig. 6). The antithetic sense of shear recorded as displacement of quartz-rich layers across the *S*-bands is also consistent with the antithetical shear expected to occur along the individual *S*-planes (Krohe, 1990). The observed pattern of *S*-band distribution between the hinge-zone and the limbs of the fold provides an explanation for how strain is accommodated in the transition zone between the flattened hinge and the sheared limbs. In addition, the oblique shear represents a departure from the geometries provided for in the flexural slip and passive folding models. Fig. 7 shows how the differences between domainal strain ellipses from a pure flexural slip and passive folding can be reconciled through the oblique shear model.

Arguments about the reduced resolved shear stress on the shear plane of a flexural slip fold with increased limb rotation have been used to discount the participation of flexural slip in folds with an interlimb angle less than 60° (e.g. de Sitter, 1958). Although speculation about the further

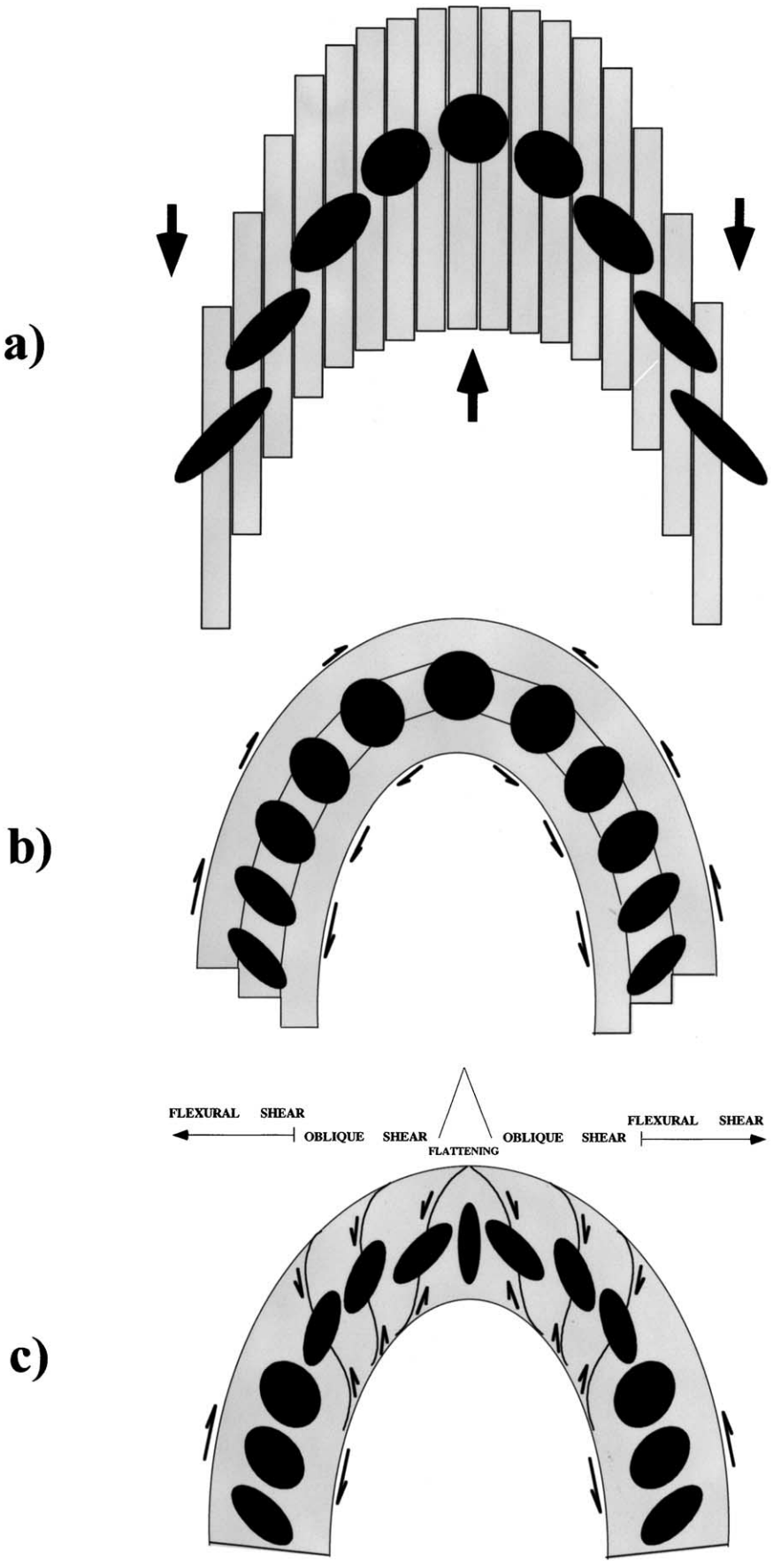
a)
b)
FLEXURAL
SHEAR
OBLIQUE
SHEAR
FLATTENING
OBLIQUE
SHEAR
FLEXURAL
SHEAR
c)

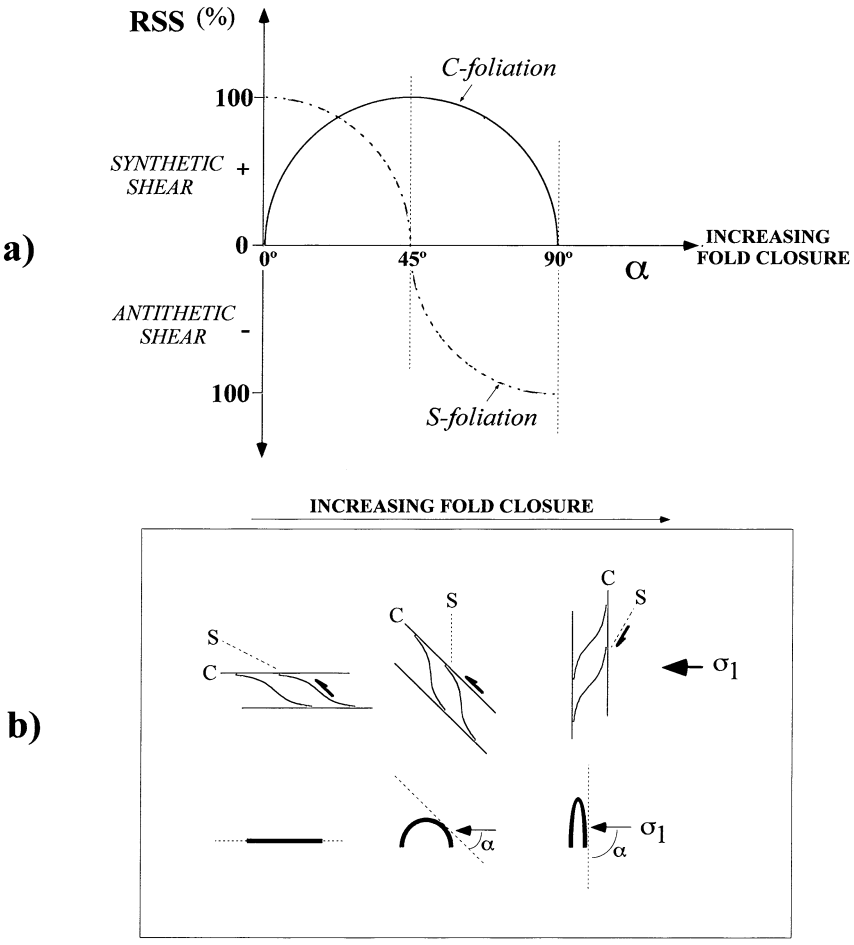

Fig. 8. (a) Diagram showing the evolving resolved shear stress (RSS) on *S*- and *C*-foliations during progressive fold closure. α is the angle between σ_1 and the fold limb. Note that after some degree of fold closure ($\alpha > 45°$), an antithetic shear (relative to the flexural shear on the *C*-foliation) is resolved on the *S*-foliation, contributing to development of oblique *S*-bands. (b) Sketch showing the position of *S*- and *C*-foliations at three different stages of fold closure ($\alpha = 0$, 45 and 90°).

development of microstructures and folding accommodation is limited by the intermediate development shown by the investigated fold (interlimb angle of 105°), we can make some estimates based on the potential for slip along oblique *S*-bands. Based on the incipient development of *S*-bands towards the inflection point of the limbs, we suggest that with increasing fold curvature the zone of oblique *S*-bands should migrate along the limbs towards the inflection point, enhancing strain accommodation, foliation development, mica enrichment and quartz depletion in these domains. At moderate to high fold curvatures (angle between limbs and $\sigma_1 > 45°$) this process should be greatly enhanced by the component of the compressional stress resolved as antithetical shear in the *S*-bands, in parallel with a decreasing resolved shear stress on the *C*-planes (Fig. 8). This process seems to lead to the same structures expected during axial-planar foliation development, where the fold hinges are the last remnants left behind during transposition by an axial plane foliation. An intriguing problem is that the shear stress resolved on the *S*-planes and *S*-bands does not contribute to the antithetical shear observed on these structures, at least at the initial stages of folding (angle between limbs and $\sigma_1 < 45°$ (Fig. 8b). Thus, all foliation formation in the limbs probably resulted from flexural slip only.

In summary, we suggest that folding in this rock was principally accommodated by two related mechanisms, flexural slip and oblique shear, both of which accommodated folding through shear along *S*–*C* foliations. A component of shortening normal to the axial plane is also inferred from the crenulation development in the hinge-zone. At the initial stages of folding, flexural slip parallel to the sedimentary layers led to development of *S*–*C* fabrics in the fold limbs. Flexural slip along the *C*-planes (which are parallel to the sedimentary layers) accounts for rotation of

Fig. 7. Comparison among the patterns of local strain ellipses produced during passive folding (a), flexural slip (b) and a combination of flexural shear in the limbs and oblique shear in the intermediate zones, which is proposed in this paper.

the limbs with respect to the stress framework during progressive fold closure. This rotation continues until the shear stress resolved across the *C*-planes become too weak to maintain *C*-planes as planes of active shear. It is at this point that antithetical oblique shear along *S*-planes becomes increasingly active. With the alignment of several *S*-plane domains and the occurrence of oblique shear along the *S*-bands, the role of *S*-planes and *C*-planes can be considered to have been fully reversed. Oblique shear, as defined here, preserves the antithetical movement along *S*-planes. However, unlike antithetical shear in ordinary *S*-planes, these oblique *S*-bands disrupt the *C*-planes, thus preserving the angle between these two planes (in the range 30–45°) produced during the initial stages of *S*–*C* fabric development in the limbs. Thus, the active shear is transferred from the *C*-planes to the *S*-planes and the folding mechanism switches from flexural slip to oblique shear.

5. Conclusions

S–*C* fabrics can accommodate folding via flexural slip at the microscopic scale. In the investigated fold, there is a gradual decrease in development of *S*–*C* fabrics towards the hinge zone. Strain in the hinge zone was accommodated by coaxial deformation reflected as crenulation development, whereas flexural slip operated in the limbs. Between the limbs and the hinge domains, there is an intermediate zone where strain was accommodated by oblique shear along *S*-bands formed by coalescence of several individual *S*-planes, which maintains the antithetical shear on these *S*-planes. However, by disrupting the *C*-planes, oblique shear on the *S*-bands prevents rotation of the *S*-planes and preserves the relatively high angles between *S*- and *C*-foliations. Continued oblique shear along these *S*-planes leads to increasing alignment and connection of individual *S*-foliations into mesoscale *S*-bands and gradual deactivation of shear along *C*-planes. Oblique shear along these *S*-bands provides a folding mechanisms which is intermediate between slip folding and flexural slip, and present some similarities with the heterogeneous pure shear folding described by Bell and Hickey (1997). Advanced stages of folding via oblique shear are speculated to lead to folds with tighter closure and also to the common development of axial plane cleavage with preserved hinge zones.

Acknowledgements

Research for this paper was made possible with funds from the Brazilian National Research Council (CNPq, process 52.3688/96-2) to J. Hippertt and a CNPq Graduate Studies Scholarship to E. Tohver. Constructive reviews were made by A. Krohe, J. Tullis, K. Hickey and S. Johnson.

References

Bell, T., 1986. Foliation development and refraction in metamorphic rocks: reactivation of earlier foliations and decrenulation due to shifting patterns of deformation partitioning. Journal of Metamorphic Geology 4, 421–444.

Bell, T., Hickey, K., 1997. Distribution of pre-folding linear indicators of movement direction around the Spring Hill synform, Vermont: significance for mechanism of folding in this portion of the Appalachians. Tectonophysics 274, 275–294.

Berthé, D., Choukrone, P., Jegouzo, P., 1979. Orthogneiss, mylonite and non-coaxial deformation of a South Armorican shear zone. Journal of Structural Geology 1, 31–42.

Borradaile, C.J., 1978. Transected folds: a study illustrated with examples from Canada and Scotland. Bulletin of the Geological Society of America 89, 481–493.

Carreras, J., Estrada, A., White, S., 1977. The effects of folding on the *c*-axis fabrics of a quartz mylonite. Tectonophysics 39, 3–24.

Chapple, W.M., Spang, J.H., 1974. Significance of layer-parallel slip during folding of layered sedimentary rocks. Bulletin of the Geological Society of America 85, 1523–1534.

Chemale, F., Rosiére, C.A., Endo, I., 1994. The tectonic evolution of the Quadrilátero Ferrífero, Minas Gerais. Precambrian Research 65, 25–54.

Davis, B., Forde, A., 1994. Regional slaty cleavage formation and foldaxis rotation by re-use and reactivation of pre-existing foliations: the Fiery Creek slate belt, North Queensland. Tectonophysics 230, 191–199.

Donath, F.A., Parker, R.B., 1964. Folds and folding. Bulletin of the Geological Society of America 75, 45–62.

Groshong Jr, R.H., 1975. Strain, fractures, and pressure solution in natural single layer folds. Bulletin of the Geological Society of America 86, 1363–1376.

Henderson, J.R., Wright, T.O., Henderson, M.N., 1986. A history of cleavage and folding: an example from the Goldenville Formation, Nova Scotia. Bulletin of the Geological Society of America 97, 1354–1366.

Hippertt, J., 1994. Microstructures and *c*-axis fabrics indicative of quartz dissolution in sheared quartzites/phyllonites. Tectonophysics 229, 141–163.

Hippertt, J., 1998. Breakdown of feldspar, volume gain, and lateral mass transfer during mylonitization of granitoid in a low metamorphic grade shear zone. Journal of Structural Geology 20, 175–193.

Hippertt, J., 1999. Are *S*–*C* structures, duplexes and conjugate shear zones different manifestations of the same scale-invariant phenomenon? Journal of Structural Geology 21, 975–984.

Hobbs, B., Muhlhaus, H.B., Ord, A., Zhang, Y., Moresi, L., 2000. Fold geometry and constitutive behaviour. In: Jessel, M., Urai, J. (Eds.). Stress, Strain and Structure, a Volume in Honour of W.D. Means. Journal of Virtual Explorer 2 (On-line at www.virtualexplorer.com.au/Vejournal/Volume2).

Hudleston, P.J., Lan, L., 1993. Information from fold shapes. Journal of Structural Geology 15, 253–264.

Hudleston, P.J., Treagus, S.H., Lan, L., 1996. Flexural flow folding: does it occur in nature? Geology 24, 203–206.

Johnson, A.M., Page, B.M., 1976. Part VII: development of folds within the Hausna syncline, San Luis Obispo County, California. Tectonophysics 33, 97–143.

Johnson, S., 1999. Porphyroblast microstructures: a review of current and future trends. American Mineralogist 84, 1711–1726.

Krohe, A., 1990. Local variations in quartz *c*-axis orientations in non-coaxial regimes and their significance for the mechanics of *S*–*C* fabrics. Journal of Structural Geology 12, 995–1004.

Law, R., Schmid, S., Wheeler, J., 1990. Simple shear deformation and quartz crystallographic fabrics: a possible natural example from the Torridon area of NW Scotland. Journal of Structural Geology 12, 29–45.

Lister, G., Paterson, M., Hobbs, B., 1978. The simulation of fabric

development in plastic deformation and its application to quartzite: the model. Tectonophysics 45, 107–158.

Lister, G., Snoke, A., 1984. *S–C* mylonites. Journal of Structural Geology 6, 617–638.

Ramsay, J.G., 1967. Folding and Fracturing of Rocks. McGraw-Hill Book Company, New York.

Ramsay, J.G., 1974. Development of chevron folds. Bulletin of the Geological Society of America 85, 1741–1754.

Ramsay, J.G., Huber, M.I., 1987. The Techniques of Modern Structural Geology Vol. 2: Folds and Fractures. Academic Press, New York.

de Sitter, L.U., 1958. Boudins and parasitic folds in relation to cleavage and folding. Geologie. Mijnb. 20, 277–288.

Starkey, J., Cutforth, C., 1978. A demonstration of the interdependence of the degree of quartz preferred orientation and the quartz content of deformed rocks. Canadian Journal of Earth Sciences 15, 841–847.

Stünitz, H., 1991. Folding and shear deformation in quartzites inferred from crystallographic preferred orientation and shape fabrics. Journal of Structural Geology 13, 71–86.

Tanner, P.W.G., 1989. The flexural slip mechanism. Journal of Structural Geology 11, 635–655.

Tanner, P.W.G., 1992. Morphology and geometry of duplexes formed during flexural-slip folding. Journal of Structural Geology 14, 1173–1192.

Treagus, S.H., Treagus, J.E., 1992. Transected folds and transpression: how are they related? Journal of Structural Geology 14, 361–367.

Twiss, R.J., 1988. Description and classification of folds in single surfaces. Journal of Structural Geology 10, 607–623.

Twiss, R.J., Moore, E.M., 1992. Structural Geology. W.H. Freeman, New York 532pp.

Williams, P., Jiang, D., 1999. Rotating garnets. Journal of Metamorphic Geology 17, 367–378.